Surface atomic and electronic structure of Mn$_5$Ge$_3$ on Ge(111)

J. Hirvonen Grytzelius,[*] H. M. Zhang, and L. S. O. Johansson

Department of Physics, Karlstad University, S-651 88 Karlstad, Sweden

(Received 17 June 2011; published 4 November 2011)

The atomic and electronic structure of the Mn$_5$Ge$_3$(001) surface grown on Ge(111) $c(2 \times 8)$ has been studied in detail by angle-resolved photoelectron spectroscopy (ARPES), scanning tunneling microscopy (STM), and scanning tunneling spectroscopy. ARPES spectra recorded from the $\bar{\Gamma}$-$\bar{K}$-$\bar{M}$ and $\bar{\Gamma}$-$\bar{M}$-$\bar{\Gamma}$ directions of the surface Brillouin zone show six surface-related features. The STM images recorded at biases higher/lower than ± 0.4 V always show a honeycomb pattern with two bright protrusions in each unit cell. At lower biases, a hexagonal, intermediate transition, and a honeycomb pattern are observed. These can be explained as arising from Mn and Ge atoms in the sublayer arranged in triangular structures and Mn atoms in the top layer arranged in a honeycomb structure, respectively. The photoemission and STM data from the germanide surface are discussed and compared to earlier published theoretical, photoelectron spectroscopy, and scanning tunneling microscopy studies.

PACS number(s): 79.60.−i, 68.35.bg, 68.35.bj

I. INTRODUCTION

New materials that exhibit both semiconducting and magnetic properties are of great interest today. In recent decades, semiconducting materials have dominated the information technology industry because their charge is easy to control; while in magnetic materials, it is instead possible to control the spin of the electron. The combination of these two types of materials will result in magnetic semiconductors exhibiting both magnetic and semiconducting properties. These materials can provide a new type of conduction control by controlling the spin transport of the electron.[1]

Magnetic materials based on Mn and Ge have received a lot of attention lately. One important fact that makes the MnGe alloy interesting is that it shows magnetic properties at a temperature of $\sim$296 K.[2] The magnetic and structural properties of thin as well as thick Mn$_5$Ge$_3$ films on Ge(111) grown by solid phase epitaxy have been studied by several groups.[2–8] Zeng *et al.*[2,3] have reported that uniform Mn$_5$Ge$_3$ films with a $\sqrt{3} \times \sqrt{3}$ periodicity, referred to as the Ge(111) surface, are produced when annealing as-deposited manganese between 300–650 °C, and that the formation of the $\sqrt{3} \times \sqrt{3}$ surface structure should be associated with the ordered Mn$_5$Ge$_3$ phase. Sangaletti *et al.*[5] provided evidence for the surface ferromagnetism in a thin metallic Mn/Ge(111) layer with a $\sqrt{3} \times \sqrt{3}$ surface structure. The low-coverage regime, i.e., the Mn/Ge interface, has also been specifically investigated.[3,9,10] Zeng *et al.*[3] reported that annealing of the as-deposited manganese at 300 °C yields a seed layer for the growth of Mn$_5$Ge$_3$. Scanning tunneling microscopy (STM) studies of solid-phase-epitaxy-grown Mn$_5$Ge$_3$ films on Ge(111) and Ge(100) have shown similar structures with the Mn$_5$Ge$_3$(0001) exposed plane.[2,3,11,12] One recurring fact in the above STM studies is that the Mn$_5$Ge$_3$ surfaces show two white protrusions in each unit cell, which are arranged in a honeycomb pattern. In theoretical-model approaches, the observed honeycomb pattern was explained by Mn atoms located on top of the Mn$_5$Ge$_3$ film. Picozzi *et al.*[13] reported theoretical calculations of the band structure for bulk Mn$_5$Ge$_3$ showing band dispersion close to the Fermi level. However, little is known about the surface band structure. So far, no detailed studies covering both angle-resolved photoelectron

spectroscopy (ARPES) and STM at low biases have been reported for the $\sqrt{3} \times \sqrt{3}$ surface structure of Mn$_5$Ge$_3$.

In this paper, we present our experimental results regarding the surface atomic and electronic structure of Mn$_5$Ge$_3$. The surface has been investigated in detail using ARPES, STM, and scanning tunneling spectroscopy (STS). The ARPES spectra from the Mn$_5$Ge$_3$ surface show six surface-related features. The STM images recorded within biases of ± 0.4 V show both a honeycomb and a hexagonal pattern. The high-quality STS spectra recorded from the Mn germanide surface are in good agreement with the ARPES data.

II. EXPERIMENTAL DETAILS

The photoemission study was performed at beam line 33 at the MAX-lab synchrotron radiation facility in Lund, Sweden.[14] The energy resolution of the angle-resolved valence-band spectra presented here is $\sim$50 meV, with an angular resolution of $\pm 2^\circ$. The STM/STS study was performed at room temperature in a variable-temperature STM system from Omicron Nanotechnology GmbH. The STM tip was made from a W wire. The pressure during evaporation was $\sim$1 × 10^{-10}, and similar during measurements. Ge(111) samples were cut from an *n*-doped (Sb, 3 Ω cm) single-crystal wafer. The Ge(111) surfaces were cleaned by repeated sputtering (Ar$^+$, 0.5 kV) and annealing cycles of 5 min at $\sim$600 °C. This procedure resulted in well-ordered $c(2 \times 8)$ surfaces, as seen by low-energy electron diffraction (LEED). Manganese was evaporated from a well-outgassed electron-beam evaporator (Omicron/Focus) at a rate of 0.5 ML/min. The evaporator was carefully calibrated by a quartz-crystal monitor. Evaporation of 32-ML manganese followed by post annealing at 450 °C resulted in an intense $\sqrt{3} \times \sqrt{3}$ LEED pattern, as seen in Fig. 1. As shown in Refs. 2 and 3, the $\sqrt{3} \times \sqrt{3}$ LEED pattern should be associated with the ordered Mn$_5$Ge$_3$ phase, since the annealing of as-deposited Mn on Ge(111) between 300–650 °C always produces uniform Mn$_5$Ge$_3$ films. Referring to these reports, we conclude that a Mn$_5$Ge$_3$ film was also produced in our case and we shall, from here on, focus on the surface atomic and electronic structure of the Mn$_5$Ge$_3$ film. It should also be noted that the Mn$_5$Ge$_3$ surface structure is slightly

FIG. 1. LEED image of the Mn_5Ge_3 surface. The sample temperature was 100 K and the primary energy of the electrons was 46 eV. The intense $\sqrt{3}$-diffraction spots are clearly seen.

larger than the $\sqrt{3}$ surface reconstruction of Ge(111). Our STM measurements showed that the lattice parameter of the Mn_5Ge_3 surface is ~2.8% larger than the lattice parameter of Ge(111)-$\sqrt{3} \times \sqrt{3}$. This is similar to bulk Mn_5Ge_3 (with a 3.7% difference).[2]

The work function has been determined by measuring the total width of the valence-band spectra from the low-energy cutoff to the Fermi level (E_F) at a photon energy of 21.2 eV and a sample bias of -9.01 V. The value obtained for the Mn_5Ge_3 surface is 4.07 eV. This is quite similar to the work function of polycrystalline Mn (4.1 eV),[15] but quite different compared to the work function for Ge(111) $c(2 \times 8)$ (4.7 eV).

III. RESULTS AND DISCUSSION

Figures 2(a) and 2(b) show two sets of angle-resolved photoemission spectra from the Mn_5Ge_3 surface recorded at 100 K along the $\bar{\Gamma}$-$\bar{M}$-$\bar{\Gamma}$ and $\bar{\Gamma}$-$\bar{K}$-$\bar{M}$ lines of the surface Brillouin zone (SBZ). The spectra show a clear metallic character, as seen by the sharp Fermi edge. In the $\bar{\Gamma}$-$\bar{K}$-$\bar{M}$ direction, six surface-related features are observed and are labeled S_1–S_6. In the $\bar{\Gamma}$-$\bar{M}$-$\bar{\Gamma}$ direction, six surface-related features are also observed, which can be correlated with the surface states observed in the $\bar{\Gamma}$-$\bar{K}$-$\bar{M}$ direction. The surface-related features discussed here may be related to both the Mn germanide surface and the "bulk" of the Mn germanide film.

In both the $\bar{\Gamma}$-$\bar{M}$-$\bar{\Gamma}$ and $\bar{\Gamma}$-$\bar{K}$-$\bar{M}$ directions, the S_1 feature is resolved at emission angles from $0°$ to $42°$. With higher emission angles, S_1 becomes less intense in both directions. The surface state S_2 appears as a small shoulder at every emission angle between $0°$ and $42°$ in the $\bar{\Gamma}$-$\bar{M}$-$\bar{\Gamma}$ and $\bar{\Gamma}$-$\bar{K}$-$\bar{M}$ directions. The surface state S_3 is also observed at emission angles between $0°$ and $42°$ in both the $\bar{\Gamma}$-$\bar{M}$-$\bar{\Gamma}$ and $\bar{\Gamma}$-$\bar{K}$-$\bar{M}$ directions. In the $\bar{\Gamma}$-$\bar{M}$-$\bar{\Gamma}$ direction, S_4 only shows up at $16°$ and $18°$. In the $\bar{\Gamma}$-$\bar{K}$-$\bar{M}$ direction, S_4 shows up between $22°$ and $38°$. In addition, the surface state S_5 is well resolved in both the $\bar{\Gamma}$-$\bar{M}$-$\bar{\Gamma}$ and the $\bar{\Gamma}$-$\bar{K}$-$\bar{M}$ directions. In the $\bar{\Gamma}$-$\bar{K}$-$\bar{M}$ direction, S_5 is most intense between $18°$ and $32°$ and then
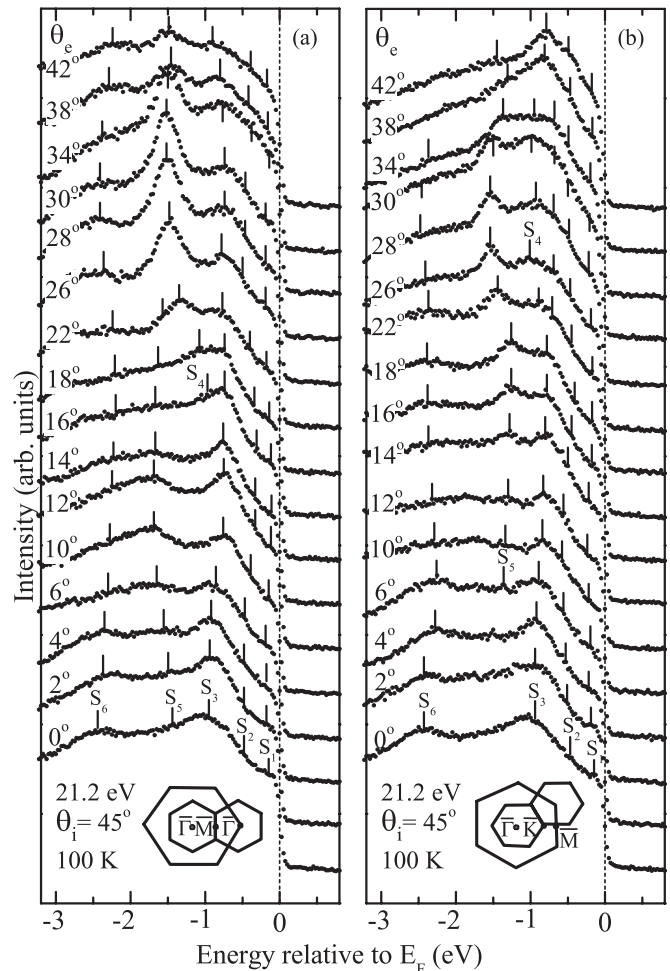
FIG. 2. ARPES spectra with various emission angles recorded at 100 K along the (a) $\bar{\Gamma}$-$\bar{M}$-$\bar{\Gamma}$ and (b) $\bar{\Gamma}$-$\bar{K}$-$\bar{M}$ line of the surface Brillouin zone. The photon energy was 21.2 eV and the incidence angle for the photons was $45°$. The six surface states are clearly observed and labeled as S_1–S_6. The inset shows the SBZ of the surface [same as the $\sqrt{3} \times \sqrt{3}$ surface of Ge(111)] together with the 1×1 SBZ of Ge(111).

it becomes less intense with higher emission angles. In the $\bar{\Gamma}$-$\bar{M}$-$\bar{\Gamma}$ direction, S_5 is most intense between $22°$ and $38°$. The sixth surface state S_6 is weak in intensity over the whole angular range in the $\bar{\Gamma}$-$\bar{M}$-$\bar{\Gamma}$ direction. In the $\bar{\Gamma}$-$\bar{K}$-$\bar{M}$ direction, S_6 is resolved between $0°$ and $34°$.

The k-resolved energy dispersion $E(k)$ of these states is displayed in Fig. 3, where the main part is obtained from the spectra in Figs. 2(a) and 2(b). The solid line displays the edges of the projected bulk band structure of the substrate, adapted from Ref. 16. At the $\bar{\Gamma}$ point, S_1 is located 0.15 eV below the Fermi level and has a bandwidth of 0.13 eV. S_1 forms a continuous band as it is resolved at every $k_{||}$ point in both the $\bar{\Gamma}$-$\bar{M}$-$\bar{\Gamma}$ and $\bar{\Gamma}$-$\bar{K}$-$\bar{M}$ directions. S_1 follows the surface periodicity since it has a local maximum at the $\bar{M}$ point and first and second $\bar{\Gamma}$ points in the $\bar{\Gamma}$-$\bar{M}$-$\bar{\Gamma}$ direction, and in the $\bar{\Gamma}$-$\bar{K}$-$\bar{M}$ direction, it has two local maxima at the first and second $\bar{K}$ points. The surface state S_2 is located 0.47 eV below the Fermi level at the $\bar{\Gamma}$ point and has a bandwidth of 0.29 eV. In both directions, it roughly follows the surface periodicity. S_3 is
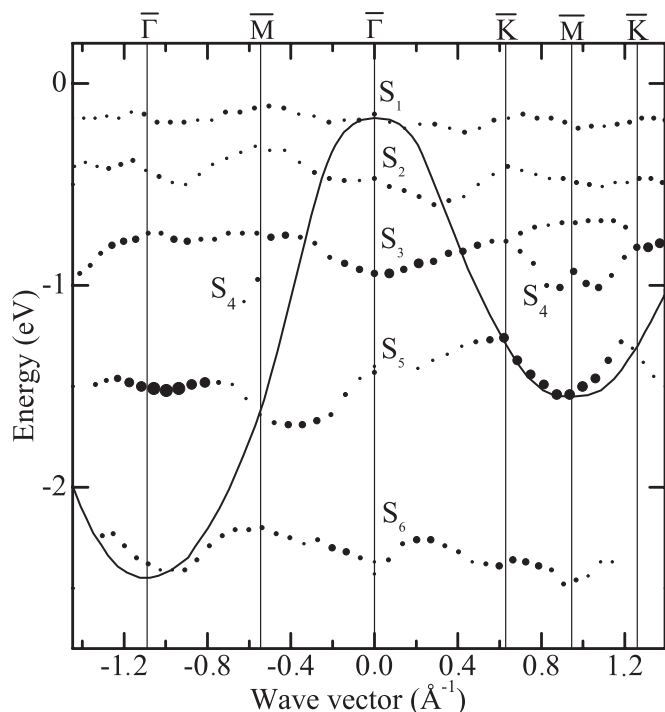
FIG. 3. Band-mapping scheme showing the dispersion of the surface states along the $\bar{\Gamma}$-$\bar{M}$-$\bar{\Gamma}$ and the $\bar{\Gamma}$-$\bar{K}$-$\bar{M}$ directions of the surface Brillouin zone. Parts of the original spectra are shown in Figs. 2(a) and 2(b). The spot size represents the intensity of the states at different emission angles. The surface states are labeled S_1–S_6. The solid line displays the upper edge of the projected bulk bands from the substrate, according to Hatta et al.[16]

located 0.94 eV below the Fermi level at the $\bar{\Gamma}$ point and has a bandwidth of 0.31 eV. In the $\bar{\Gamma}$-$\bar{K}$-$\bar{M}$ direction, one additional surface feature shows up between the first and second $\bar{K}$ points with a binding energy of -1.0 eV. We tentatively assign it as a surface state, denoted S_4. A similar feature is found near the $\bar{M}$ point in the $\bar{\Gamma}$-$\bar{M}$-$\bar{\Gamma}$ direction, probably arising from the same state, as they are located at similar binding energies at the two $\bar{M}$ points. Surface state S_5 is located 1.4 eV below the Fermi level at the first $\bar{\Gamma}$ point. In the $\bar{\Gamma}$-$\bar{K}$-$\bar{M}$ direction, S_5 has two local maxima at the $\bar{K}$ points and one local minimum at the $\bar{M}$ point. Evidently, S_5 follows the periodicity of the surface Brillouin zone. The bandwidth of S_5 is 0.45 eV. S_6 is located 2.4 eV below the Fermi level at the $\bar{\Gamma}$ point. The band dispersion of S_6 is 0.28 eV.

In earlier PES studies, two broad peaks were observed, with one close to the Fermi edge and one about 2.5 eV below the Fermi level. These two states were assigned to the Mn $3d$ states.[5] Comparing our ARPES spectra with the previous data, one finds that the state close to the Fermi level in Ref. 5 consists of three states, S_1–S_3; that is, two weak states located at 0.15 and 0.47 eV, and one at 0.94 eV below the Fermi level. Since these three states are located rather close to each other, they might appear as a broad peak in an angle-integrated PES spectrum. The second broad peak in Ref. 5 is similar to the surface state S_6, as they are located at a similar binding energy below the Fermi level. The surface-related feature S_5 located at binding energy 1.4 eV below the Fermi level could appear as a tail toward a lower binding energy in the PES spectrum in Ref. 5.

The resulting bands (S_1, S_2, and S_3) from photoemission will be discussed together with the STM/STS data and the atomic model. In the band structure calculation in Ref. 13, the authors assigned states between -1 and -2 eV to Mn_I-Mn_{II} interactions, and states between -2 and -3 eV to Mn_I-Mn_I interactions. In our case, S_5 and S_6 are located at -1.5 and -2.4 eV below the Fermi level. Thus, S_5 and S_6 find their natural origins in terms of the Mn_I-Mn_{II} and Mn_I-Mn_I interactions, respectively.

The surface states of the Mn_5Ge_3 surface show up to be much alike the surface states of Mn/Si(111)-$\sqrt{3} \times \sqrt{3}$ in Ref. 17. In that study, the surface states S_1–S_4 show similar energy positions and dispersions as S_1–S_4 in this study. However, there are some differences, especially in the binding energies of S_5 and S_6. In the Mn/Si(111)-$\sqrt{3} \times \sqrt{3}$ case, there is one additional surface state, S_5, located about 1.95 eV below the Fermi level. The Mn_5Ge_3 surface has two additional surface states, S_5 and S_6. In addition to the surface termination, the differences between these two electronic structures might be related to the film thicknesses, i.e., in the Mn/Si(111)-$\sqrt{3} \times \sqrt{3}$ case, 3-ML Mn was evaporated to form the Mn silicide, while in the Mn_5Ge_3 case, 32-ML Mn was evaporated to form a full-coverage Mn germanide. To get more conclusive information about the surface atomic and electronic structures, a detailed STM/STS investigation has also been done in this study.

Figures 4(a) and 4(b) show an atomic model of Mn_5Ge_3, according to Forsyth et al.[18] In this model, the unit cell of Mn_5Ge_3 along the [001] crystallographic direction possesses four atomic layers stacked along the z direction (with $z = 1$ defined as one unit cell length). Two layers containing only Mn atoms and labeled Mn_I are located at $z = 0$ and $z = 1/2$. The other two layers contain equal amounts of Mn (Mn_{II})
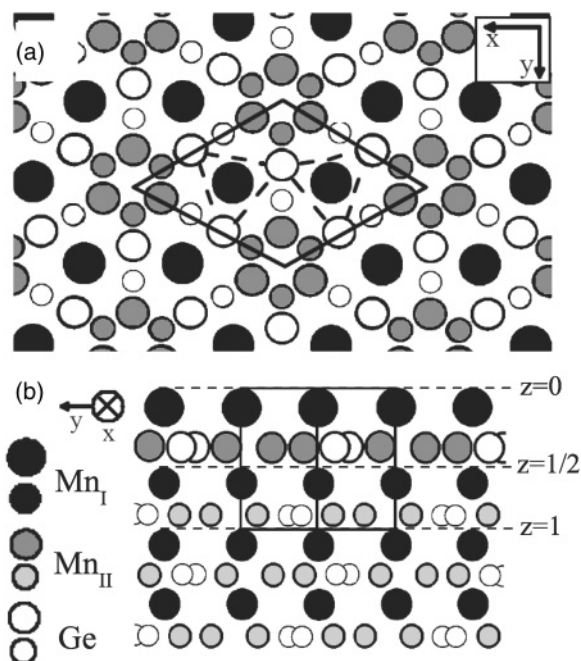
FIG. 4. The atomic structure of Mn_5Ge_3 (according to Ref. 18) (a) in top view and (b) cross section. The black rhombus and square indicate the unit cell location.
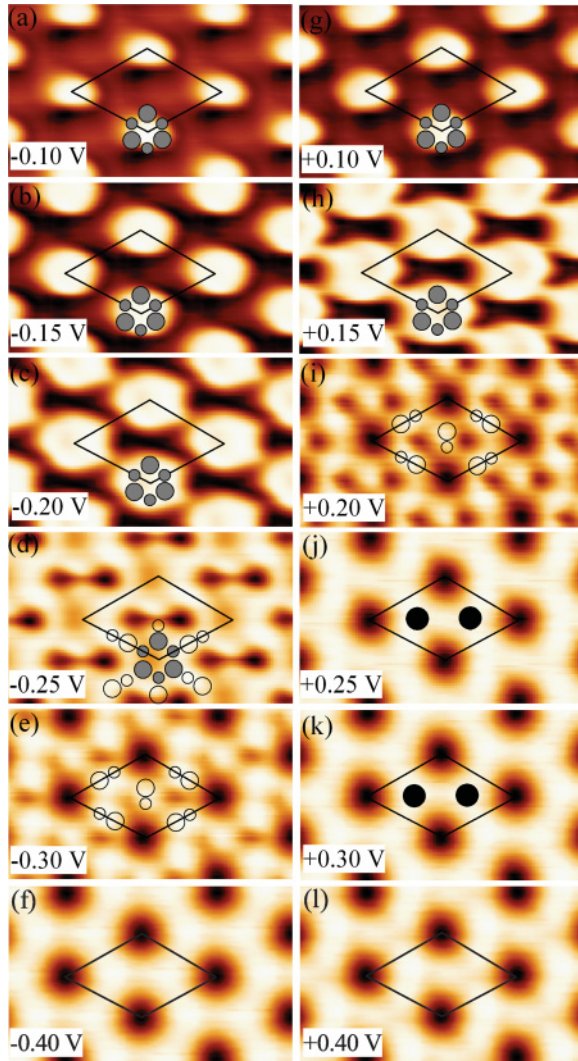
FIG. 5. (Color online) STM images from the Mn_5Ge_3 surface. (a)–(f) Filled-state images recorded at $V_S = -0.1$ to -0.30 V, $I = 25$ pA. (g)–(l) Empty-state images from the same area as in (a)–(f), $V_S = 0.1$ to 0.3 V, $I = 25$ pA. The size of the images is 2.4×1.4 nm. The black rhombus in all images indicates the unit cell. Circles in the figures indicate possible atom locations at the different biases.

in the first mixed MnGe layer [see Fig. 4(b) for a cross section of the atomic model]. At -0.30 V, the white protrusions split into three smaller elongated spots located at the sides of the unit cell. When comparing to the model in Fig. 4(a), we find both the ringlike structure and the split white protrusions fits well into the model. At -0.40 V, bright white protrusions are arranged in a typical honeycomb pattern that is common for the Mn_5Ge_3 surface. Here, the corners of the unit cell show weak electronic states; instead, an intense honeycomb pattern is observed with bright white protrusions at the locations of Mn_I atoms, according to the model in Figs. 4(a) and 4(b).

Figures 5(g)–5(l) show the empty-state images recorded from the Mn_5Ge_3 surface. At $+0.1$ V, the protrusions are arranged in a typical hexagonal pattern similar to the the filled-state image recorded at -0.1 V. With higher biases, the white protrusions evolve in the same way as in the filled-state images. That is, from hexagonal to triple split protrusions and, finally, into a honeycomb pattern. Thus the empty-state STM images look like the mirror parts of the filled-state images, especially in the lower bias range. It should also be noted that at biases higher than $+0.4$ eV and lower than -0.4 eV ($I_t = 25$ pA), the honeycomb pattern is always observed.

From -0.30 to $+0.20$ V, the evolution of the white protrusions could be explained by Mn_{II} atoms located around the corners of the unit cell, and by Ge atoms located at the side of the unit cell, as shown in the atomic model in Fig. 4(a). The honeycomb pattern observed at higher/lower voltages cannot be explained straightforwardly in terms of a mixed Mn/Ge layer only. In Refs. 3 and 12, they showed by different theoretical approaches that the Mn_5Ge_3 surface is terminated with Mn atoms arranged in a honeycomb pattern. However, in earlier studies, there exists no clear experimental evidence for a terminating Mn layer, which leaves an open question.

A common feature for the Mn_5Ge_3 surface is point defects. They appear as threefold black holes in both filled- and empty-state images; see, for example, Figs. 8(a) and 8(b) in Ref. 3. The point defect indicates that an atom is missing in the surface structure. Also in our STM study, we observed the threefold point defects at sample biases higher than $+0.35$ eV and lower than -0.35 eV. Figure 6(a) is an empty-state image recorded
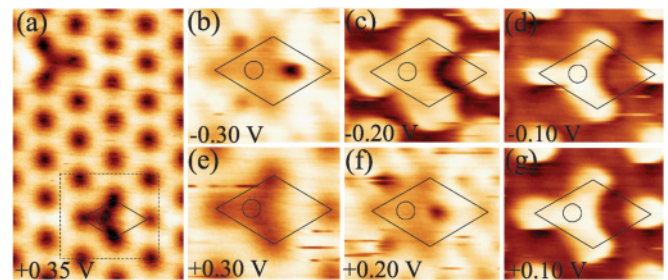
FIG. 6. (Color online) Topographic STM images recorded from the Mn_5Ge_3 surface. (a) The honeycomb pattern with two point defects, 5.0×3.2 nm, $V_S = +0.35$ V, $I = 25$ pA. (b)–(d) Filled-state images recorded from one of the defects in (a), $V_S = -0.30$ to -0.10 V, $I = 25$ pA. (e)–(g) Empty-state images recorded from the same area as in (b)–(d), $V_S = +0.30$ to $+0.10$ V, $I = 25$ pA. The size of (b)–(g) is 2.2×1.5 nm. The rhombus indicates the unit cell and the circle is the location of a missing atom.

and Ge atoms, and are located at $z = 1/4$ and $z = 3/4$. In the model, there are two possible surface terminations: a Mn-only layer or a mixed Mn/Ge layer. Earlier reports regarding the surface structure of Mn_5Ge_3 suggested that it is terminated by Mn atoms (Mn_I).[2–6,8] This will be discussed in detail below.

Figures 5(a)–5(f) show the filled-state images from the Mn_5Ge_3 surface. In the image recorded at -0.1 V, the white protrusions form a typical hexagonal pattern and are concentrated around the corners of the unit cell. With a bias of -0.15 V, the white protrusions becomes more intense and larger, and at -0.20 V, they show a smaller intensity at the center of the white protrusions. As a matter of fact, the protrusions show a higher intensity in a ringlike structure around the corners of the unit cell. This ringlike structure becomes even clearer at -0.25 V. At this bias, the image most likely shows the hybridization between the Mn_{II} and Ge atoms

at +0.35 V and shows a typical honeycomb pattern with two white protrusions in the unit cell. One of the point defects, indicated with a square, has been studied in detail.

Figures 6(b)–6(d) show the filled-state images and Figs. 6(e)–6(g) show the empty-state images recorded from the point defect in the surface structure. In each of the images, the black rhombus indicates the unit cell and the circle is the location of the missing white protrusion at +0.35 V. In the filled-state image recorded at −0.30 V, the left side of the unit cell loses its splitting and shows weakly distributed intensities, instead of three elongated white protrusions as in Fig. 5(e). Also in the empty-state images, the left side of the unit cell shows weakly distributed intensities. Interestingly, the contrast in the images recorded at biases close to the Fermi level (showing a hexagonal pattern) is the opposite compared to the images at biases higher than +0.35 eV and lower than −0.35 eV (showing a honeycomb pattern). The behavior of the point defect could be explained if one assumes a missing Mn_I atom, since it has a threefold symmetry.

One commonality in both the empty- and filled-state images (Fig. 6) is that with voltages closer to the Fermi level (0 V), the protrusions at the circle positions become more pronounced. At low bias, the Mn_I atoms are not visible and only the subsurface structures show up. Removing one top Mn_I atom makes the Ge trimer [Fig. 4(a)] visible at that position. Also it is likely that the wave functions from the surrounding Mn_{II} try to fill the hole caused by the missing Mn_I atom. The above two effects could explain why the missing Mn_I gives rise to a bright contrast at lower biases. If the point defect was a missing Mn_{II} atom, it should appear in another configuration; there should be a defect located close to a corner in the unit cell (the bright protrusions in the hexagonal pattern). To summarize this part, at low biases the surface structure could be described without the top Mn, but at higher biases the extra layer is needed to completely describe the surface atomic structure of Mn_5Ge_3-Ge(111). The above discussions support the assumption of a terminating Mn top layer.

It is interesting to compare our STM and ARPES results to the earlier STM studies.[2,3,11,12] Kim *et al.*[11] showed in their STM study a strong bias dependence for the Mn_5Ge_3 surface. Their STM images obtained at sample biases of ±0.5 eV [Figs. 3(c) and 3(d) in Ref. 11] showed in the filled-state image a dot-array arrangement, which was associated with either the Mn_{II} or the Ge atoms in the mixed Mn/Ge subsurface layer. In the empty-state image, a ring array structure was observed and associated with the Ge atoms in the mixed Mn/Ge subsurface.

Our high-resolution STM images recorded at low biases show the mixed Mn/Ge subsurface in detail i.e., both Mn_{II} and Ge atoms are observed in both empty- and filled-state images. With the aid of the atomic models shown in Figs. 4(a) and 4(b), we find that the Ge atoms are observed in the images recorded at −0.30 and +0.20 V, in which the bright protrusions are arranged in two equivalent triangles in each unit cell [dashed lines in Fig. 4(a)]. This is also supported by the DFT simulated empty-state image shown in Fig. 8(f) in Ref. 3 and in the Tersoff-Hamann approximated images in Fig. 4(f) in Ref. 12, both of which show the same triangular structures. The filled-state image recorded at −0.25 V [Fig. 5(d)] shows a clear ringlike structure, which can be explained by the Mn_{II} and Ge hybridized state in the mixed Mn/Ge subsurface. At smaller
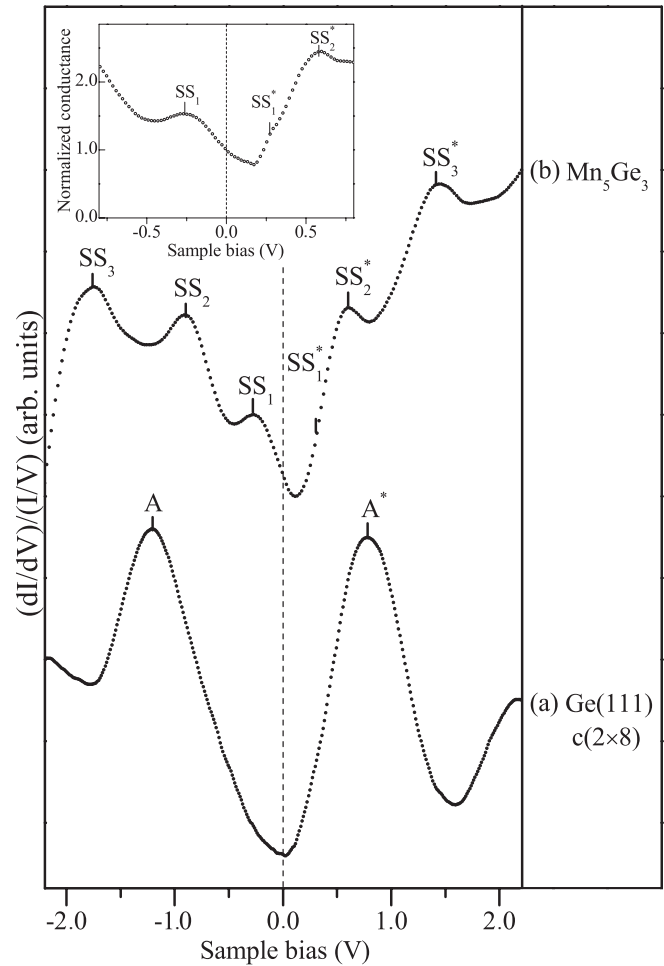
FIG. 7. Area-averaged STS spectra recorded from the (a) clean Ge(111) $c(2\times8)$ surface and (b) Mn_5Ge_3 surface. STS spectra (numerical derivatives) were obtained within biases ±2.5 V, setpoint voltage $V_S = 1.5$ V, and tunneling current $I_t = 50$ pA.

biases, close to 0 V, the white protrusions are concentrated around the Mn_{II} atoms. The Mn_{II} structure in the model appears as dense triangles around the corners of the unit cell. A dense trianglelike structure is often observed as one bright protrusion in STM; see, for example, Refs. 19 and 20. In contrary to Ref. 11, it is rather clear that the triangular structures in the STM images should be associated with the Ge atoms in the mixed Mn/Ge layer and not with the Mn_{II} atoms.

Figure 7 shows area-averaged STS spectra recorded from the clean Ge(111) $c(2 \times 8)$ sample and the sample with the 32-ML Mn germanide. In the spectrum from the $c(2 \times 8)$ surface, two intense states are observed located at −1.20 and +0.81 V. The state observed at −1.20 V is most likely the occupied states from the adatom and backbond states. It should be noted that the slow decrease in intensity from −1.2 V towards 0 V is most likely caused by the occupied states from the two different rest atoms in the Ge(111) $c(2 \times 8)$ atomic structure.[21] The state located at +0.81 V is associated with the unoccupied adatom states.

Spectrum (b) in Fig. 7 shows the area-averaged STS spectrum from the Mn_5Ge_3 surface. Five distinct surface states and one small shoulder are observed. Three occupied states

labeled SS_1–SS_3 are located at -0.25, -0.90, -1.80 eV below the Fermi level and three unoccupied states labeled as SS_1^*–SS_3^* are located at $+0.25$, $+0.55$, and $+1.4$ eV above the Fermi level. To be sure of the existence of SS_1^*, the electronic states close to the Fermi level were measured in more detail (see inset in Fig. 7). As expected, the spectrum is repeated but with a clearer shoulder at $+0.25$ eV. Thus the empty states also look like the mirror parts of the filled states.

In agreement with the ARPES data, the STS spectrum from the germanide surface shows a clear metallic character. This can easily be seen in the inset in Fig. 7, where the $(dI/dV)/(I/V)$ curve approaches 1 near zero bias.

The occupied surface state SS_1 is very broad, from 0 to -0.5 eV, and is most likely the integrated contribution from both S_1 and S_2 observed in the k-resolved energy dispersion of the surface states in Fig. 3. Usually an STS spectrum is comparable to an angle-integrated PES spectrum and does not show detailed information about the dispersion of surface states. Instead, an integrated signal covering the bandwidth of the surface states is recorded and appears as a broad feature in the spectrum. By comparing the energy position of SS_1 to S_1 and S_2, one finds that it is located in the middle between S_1 and S_2. Thus SS_1 is most likely the integrated contribution from these two surface-state bands. From the filled-state STM images, we associate the surface states S_1 and S_2 to Mn_{II} and Ge, respectively.

The surface state SS_2 is comparable to S_3 since they are located at similar binding energies. Most likely, the surface state S_3 should be associated with the Mn_I atoms on top of the surface. This can also be supported by the fact that in the topographic STM images recorded at biases higher than 0.40 eV and lower than -0.40 eV, a honeycomb pattern is observed, in which the two white protrusions are located at the positions with Mn_I atoms.

IV. CONCLUSION

In the ARPES study, six surface-related features are found in both the $\bar{\Gamma}$-$\bar{K}$-$\bar{M}$ and $\bar{\Gamma}$-$\bar{M}$-$\bar{\Gamma}$ directions of the SBZ. The STM images from the Mn_5Ge_3 surface show a hexagonal, intermediate transition, and a honeycomb pattern, depending on the sample biases. These patterns are interpreted as arising from Mn and Ge atoms in the second layer arranged in triangular structures, and Mn atoms in the top layer arranged in a honeycomb structure, respectively. High-quality STS spectra have been presented for the Mn germanide. The features observed in the STS spectra for the Mn_5Ge_3 surface show clear mirrored empty and filled states. The filled states could be associated with the surface-state bands in the ARPES study. The results from our ARPES, STM, and STS studies have given important new information about the surface electronic structure of the Mn_5Ge_3 surface.

ACKNOWLEDGMENTS

*Joakim.Hirvonen@kau.se

[1] S. A. Wolf, D. D. Awschalom, R. A. Buhrman, J. M. Daughton, S. von Molnar, M. L. Roukes, A. Y. Chtchelkanova, and D. M. Treger, Science **294**, 1488 (2001).

[2] C. Zeng, S. C. Erwin, L. C. Feldman, A. P. Li, R. Jin, Y. Song, J. R. Thompson, and H. H. Weitering, Appl. Phys. Lett. **83**, 24 (2003).

[3] C. Zeng, W. Zhu, S. C. Erwin, Z. Zhang, and H. H. Weitering, Phys. Rev. B **70**, 205340 (2004).

[4] L. Sangaletti, D. Ghidoni, S. Pagliara, A. Goldoni, A. Morgante, L. Floreano, A. Cossaro, M. C. Mozzati, and C. B. Azzoni, Phys. Rev. B **72**, 035434 (2005).

[5] L. Sangaletti, E. Magnano, F. Bondino, C. Cepek, A. Sepe, and A. Goldoni, Phys. Rev. B **75**, 153311 (2007).

[6] Y. S. Dedkov, M. Holder, G. Mayer, M. Fonin, and A. B. Preobrajenski, J. Appl. Phys. **105**, 073909 (2009).

[7] R. P. Panguluri, C. Zeng, H. H. Weitering, J. M. Sullivan, S. C. Erwin, and B. Nadgorny, Phys. Status Solidi B **242**, R67 (2005).

[8] P. De Padova, J.-M. Mariot, L. Favre, I. Berbezier, B. Olivieri, P. Perfetti, C. Quaresima, C. Ottaviani, A. Taleb-Ibrahimi, P. Le Fèvre, F. Bertran, O. Heckmann, M. C. Richter, W. Ndiaye, F. D'Orazio, F. Lucari, C. M. Cacho, and K. Hricovini, Surf. Sci. **605**, 638–643 (2011).

[9] A. Verdini, A. Cossaro, L. Floreano, A. Morgante, A. Goldoni, A. Sepe, S. Pagliara, and L. Sangaletti, Surf. Sci. **600**, 4369 (2006).

[10] A. Verdini, A. Cossaro, L. Floreano, A. Morgante, A. Goldoni, D. Ghidoni, A. Sepe, S. Pagliara, and L. Sangaletti, Phys. Rev. B **77**, 075405 (2008).

[11] H. Kim, G. -E. Jung, J. K. Yoon, K. H. Chung, and S. -J. Kahng, Surf. Sci. **602**, 481 (2008).

[12] H. Kim, G. -E. Jung, J. -H. Lim, K. H. Chung, S. -J. Kahng, W. -J. Son, and S. Han, Nanotech. **19**, 025707 (2008).

[13] S. Picozzi, A. Continenza, and A. J. Freeman, Phys. Rev. B **70**, 235205 (2004).

[14] B. N. Jensen, S. M. Butorin, T. Kaurila, R. Nyholm, and L. I. Johansson, Nucl. Instrum. Methods Phys. Res. A **394**, 243 (1997).

[15] D. E. Eastman, Phys. Rev. B **2**, 1 (1970).

[16] S. Hatta, T. Aruga, C. Kato, S. Takahashi, H. Okuyama, A. Harasawa, T. Okuda, and T. Kinoshita, Phys. Rev. B **77**, 245436 (2008).

[17] J. Hirvonen Grytzelius, H. M. Zhang, and L. S. O. Johansson, Phys. Rev. B **78**, 155406 (2008).

[18] J. B. Forsyth and P. J. Brown, J. Phys. Condens. Matter **2**, 2713 (1990).

[19] J. Hirvonen Grytzelius, H. M. Zhang, and L. S. O. Johansson, Phys. Rev. B **80**, 235324 (2009).

[20] H. M. Zhang, J. B. Gustafsson, and L. S. O. Johansson, Phys. Rev. B **74**, 201304(R) (2006).

[21] I. Razado-Colambo, Jiangping He, H. M. Zhang, G. V. Hansson, and R. I. G. Uhrberg, Phys. Rev. B **79**, 205410 (2009).